Implementing positive-operator-valued-measurement elements in photonic circuits for performing minimum quantum state tomography of path qudits

W. R. Cardoso,* D. F. Barros, M. R. Barros, and S. Pádua
Departamento de Física, Universidade Federal de Minas Gerais, 31270-901 Belo Horizonte, Minas Gerais, Brazil

(Received 22 December 2018; published 20 June 2019)

Manipulation of qudits in optical tables is a difficult and nonscalable task. The use of integrated optical circuits opens new possibilities for the generation, manipulation, and characterization of high dimensional states besides the ease of transmission of these states through an optical fiber. In this work we propose photonic circuits to perform minimum quantum state tomography of path qudits and show how to determine all the constituents parameters of these circuits (beam splitters and phase shifters). Our strategies were based on the symmetries of the involved POVMs (positive operator-valued measures) suggested for minimum tomography and allowed us to obtain interferometers smaller than those obtained by other already known methods. The calculations of the transmittances and reflectivities of the beam splitters were made using the definition of probability operators in extended Hilbert spaces and the application of Naimark's theorem. The employment of equidistant states for the definition of the POVM elements allowed us to develop a recipe applicable to the tomography of qudits of any dimension, generalizing our scheme.

DOI: 10.1103/PhysRevA.99.062324

I. INTRODUCTION

A qubit corresponds to the fundamental unit of quantum information in the same sense as the bit corresponds to the fundamental classical unit of information. When we are referring to quantum states with a Hilbert space with dimension $N > 2$, then we speak of *qudits* [1–6]. The use of qudits opens new prospects for quantum information processing, such as the enhancement of security for quantum key distribution, the increase of channel capacity, higher noise resistance, and quantum computing [7–19].

Manipulating states of qudits in interferometers at optical tables is a nonscalable and challenging task. Interferometers have been set for characterizing quantum states [20–24], controlling, detecting, or measuring entanglement of qudit systems [9,10,25,26], or simulating noisy channels [27,28]. The use of photonic circuits written in glasses by a femtosecond direct laser writing technique opens new possibilities for the generation, manipulation, and characterization of high dimensional states, besides the direct transmission of these states through an optical fiber [29–36]. Using longitudinal interferometers, we can implement quantum operations in two qudits states, including transforming them from antisymmetric states to symmetric ones, making it possible to construct interferometers for simulation of open systems and their characterization [37–40]. Remote preparation of arbitrary qudits for their use in quantum communication protocols is another possible application for these circuits [41–44].

Recently, the generation and analysis of a two qutrits system in a silicon photonic circuit generated with the lithographic technique was demonstrated [45]. In this domain, we can use such a result to produce states of two qudits from an integrated photonic chip drawn on glass, after they receive photon pairs generated by spontaneous parametric down-conversion (SPDC). We aim here the construction of photonic circuits that, by implementing POVM (positive operator-valued measure) elements, are able to perform minimum full quantum state tomography of qudits, defined as an experimental technique that allows the reconstruction of the density matrix of a quantum system in an unknown state with a minimum number of measurements [46–50]. These techniques satisfy a demand in current computer and telecommunications technologies: the ability to execute quantum information protocols on small devices that integrate a larger hardware design. Our accomplishment is a contribution in the development of quantum information tasks in chips. It contributes to the technology needed to reach compact and portable devices for quantum protocols.

Quantum state tomography on a chip has been a subject of interest to various research groups. It demonstrated, theoretically and experimentally, the accomplishment of quantum tomography in photonic chips through quantum walks [51,52]. The authors used in their experiment a circuit with N inputs and M outputs to characterize a photon-number state. The detection of the photons of all the outputs is done simultaneously, optimizing the experiment duration. Since it is not necessary to reconfigure the experimental apparatus, the occurrence of errors is also reduced. Circuits that do not require reconfiguration are called static circuits [53].

In this work we present an alternative form of performing full quantum tomography on photonic chips, by the implementation of POVM elements in static circuits, whose detection at all outputs is made simultaneously. All necessary POVM elements are implemented at the same time by the circuit and measured at the different photonic circuit exits simultaneously. All necessary measurement probabilities are obtained from the photon counts at the circuit outputs in

*will.rodrigues.fis@gmail.com

one measurement time interval. This is important because it minimizes the noise introduced by the experimental apparatus during the detection time. The proposed tomography method uses SIC-POVM (symmetric informationally complete positive operator-valued measure) elements, allowing a full quantum state tomography with the minimum number of measurements and with a symmetric POVM elements distribution in Hilbert space that optimizes the system density operator reconstruction [21,54–58].

Our proposal is based on the application of Naimark's theorem. The POVM cannot be realized by an unitary transformation followed by a projective measurement in the original qudit space. Therefore, the initial qudit Hilbert space is expanded and the realization of the POVM elements occurs by applying unitary transformations followed by projection measurements in this extended space [59–63]. This task can be realized in multiport interferometers, composed of beam splitters and phase shifters, built by using, for example, the Reck's proposition [64]. An important advance was done by Clements *et al.* that propose a different design for the multiport interferometer that, by using the same number of components, decreases the optical depth of the interferometer [65]. This quantity is important for fabricating smaller interferometers with smaller losses.

The unitary transformations in the extended Hilbert space in our circuit design uses a smaller number of beam splitters than Reck *et al.* and Clements *et al.* general designs with a smaller optical depth, which is a clear advantage for this specific task. It is necessary to mention that the proposed circuit design realizes full quantum tomography with the minimum number of measurements and no hypothesis about the initial system state are necessary. Other schemes are able to realize quantum tomography with a number of measurements smaller than the minimum for a particular class of system states using prior knowledge of the input state [53].

Finally, the organization of the rest of the paper is as follows: in Sec. II we briefly discuss some useful concepts about minimum state tomography for qubits. After this short introduction, we present in Sec. III the proposal for construction of the tomographical circuits for this case. We then proceed in Sec. IV with the circuit's proposal in the qutrit case. In Sec. V we generalize our proposal for N dimensions. Finally, we conclude in Sec. VI.

II. MINIMUM QUANTUM STATE TOMOGRAPHY FOR QUBITS

As already mentioned in the Introduction, quantum state tomography is an experimental technique that allows the reconstruction of the density matrix of an unknown quantum system state. Its realization consists of the production of a large number of identically prepared system states together with a series of measurements of the physical quantities that it describes. When the tomography is made using the least possible number of operations, it is called a minimum full quantum state tomography [66,67]. To perform a minimal full tomography on a qubit system, one needs a POVM with four different elements $\hat{E}_j$ to be implemented in the initial state $\hat{\rho}$. The outcome's counting rate c_j is

$$c_j = AP_j, \tag{1}$$

where A is a constant proportional to the detector efficiency and the number of identically prepared states in 1 s and $P_j = \mathrm{Tr}[\hat{\rho}\hat{E}_j]$ is the probability of detecting one of the output states after E_j is implemented. By implementing these POVM elements, it is possible to determine the qubit state since the number of counts is going to be accessible.

As seen in [67], the necessary POVM elements to be implemented are

$$\hat{E}_k = \tfrac{1}{2}|\varphi_k\rangle\langle\varphi_k|, \tag{2}$$

with $k = 1, 2, 3, 4$ and

$$|\varphi_1\rangle = \omega|0\rangle + i\upsilon|1\rangle, \tag{3a}$$

$$|\varphi_2\rangle = \omega|0\rangle - i\upsilon|1\rangle, \tag{3b}$$

$$|\varphi_3\rangle = \upsilon|0\rangle - \omega|1\rangle, \tag{3c}$$

$$|\varphi_4\rangle = \upsilon|0\rangle + \omega|1\rangle, \tag{3d}$$

where $\omega = \sqrt{2/3}$ and $\upsilon = \sqrt{1/3}$. If the density operator $\hat{\rho}$ is written as $\hat{\rho} = (\hat{I} + \vec{r}\cdot\vec{\sigma})/2$, where $\vec{r} = (r_x, r_y, r_z)$ and $\vec{\sigma} = (\hat{\sigma}_x, \hat{\sigma}_y, \hat{\sigma}_z)$ is the Pauli vector, we need to determine the values of the quantities r_x, r_y, and r_z from the experimental outcome's counting rates c_j [Eq. (1)] in order to reconstruct the initial state density matrix $\hat{\rho}$. By using the POVM elements shown in Eq. (2) in Eq. (1), we obtain

$$r_x = \frac{3(c_4 - c_3)}{A\sqrt{2}}, \tag{4a}$$

$$r_y = \frac{3(c_1 - c_2)}{A\sqrt{2}}, \tag{4b}$$

$$r_z = \frac{3(c_1 + c_2 - c_3 - c_4)}{A}, \tag{4c}$$

where $A = c_1 + c_2 + c_3 + c_4$.

III. CONSTRUCTION OF THE TOMOGRAPHICAL CIRCUITS FOR QUBITS

Any unitary operator of finite size can be constructed in the laboratory using an appropriate combination of two optical devices: beam splitters (BS) and phase shifters [64]. Therefore, we can express an N-dimensional operator $\hat{U}'$ as

$$\hat{U}' = \hat{T}_n\hat{T}_{n-1}\cdots\hat{T}_2\hat{T}_1, \tag{5}$$

where $\hat{T}_j$ is an N-dimensional matrix that represents the jth operation performed on the input state and n is the number of operations required for the implementation of the matrix $\hat{U}'$. The $\hat{T}_j$ matrix is a block-diagonal matrix, where each block is composed from the elements of the BS matrix, defined as follows [64]:

$$\hat{U}_{\mathrm{BS}} = \begin{bmatrix} e^{i\phi}\sqrt{r} & e^{i\phi}\sqrt{t} \\ \sqrt{t} & -\sqrt{r} \end{bmatrix}, \tag{6}$$

in which t is the transmittance of the beam splitter and r is its reflectivity. These parameters satisfy the equation $r + t = 1$. The parameter ϕ indicates the phase difference between the outputs of the beam splitter. These are the building blocks we will use to create a scheme for minimal quantum state tomography in integrated chips.

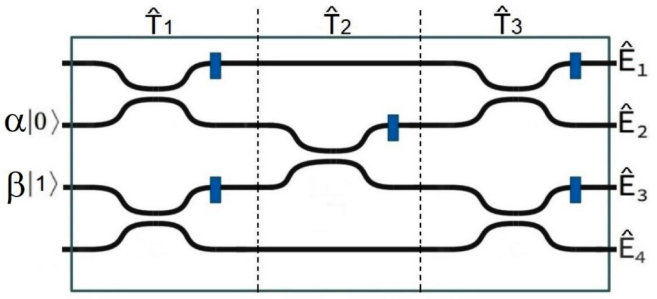

FIG. 1. Circuit proposal for the realization of the minimal state tomography on a one-qubit system. The black lines are the photon paths realized by the waveguides; the BS's are represented by the approximation of these lines and the phase shifters are the blue rectangles. This proposal was made on the assumption that the modes of the photonic qubit labeled as $|0\rangle$ and $|1\rangle$ are coupled to the second and third waveguides, respectively.

The first goal of this article is to propose a photonic circuit that implements the minimal full path state tomography on a one-qubit system. The simpler choice for the interferometer is shown in Fig. 1. In this configuration, each outcome of the interferometer corresponds to the implementation of one of the different maps $\hat{E}_k$, with $k = 1, 2, 3, 4$ [Eq. (2)], allowing us to obtain the outcomes simultaneously. The $\hat{T}_j$ operators that it constitutes (Fig. 1) are

$$\hat{T}_1 = \begin{bmatrix} e^{i\phi_1}\sqrt{r_1} & e^{i\phi_1}\sqrt{t_1} & 0 & 0 \\ \sqrt{t_1} & -\sqrt{r_1} & 0 & 0 \\ 0 & 0 & e^{i\phi_2}\sqrt{r_2} & e^{i\phi_2}\sqrt{t_2} \\ 0 & 0 & \sqrt{t_2} & -\sqrt{r_2} \end{bmatrix}, \tag{7}$$

$$\hat{T}_2 = \begin{bmatrix} 1 & 0 & 0 & 0 \\ 0 & e^{i\phi_3}\sqrt{r_3} & e^{i\phi_3}\sqrt{t_3} & 0 \\ 0 & \sqrt{t_3} & -\sqrt{r_3} & 0 \\ 0 & 0 & 0 & 1 \end{bmatrix}, \tag{8}$$

$$\hat{T}_3 = \begin{bmatrix} e^{i\phi_4}\sqrt{r_4} & e^{i\phi_4}\sqrt{t_4} & 0 & 0 \\ \sqrt{t_4} & -\sqrt{r_4} & 0 & 0 \\ 0 & 0 & e^{i\phi_5}\sqrt{r_5} & e^{i\phi_5}\sqrt{t_5} \\ 0 & 0 & \sqrt{t_5} & -\sqrt{r_5} \end{bmatrix}. \tag{9}$$

Since we need to expand the Hilbert space, we will use as an initial state $|\psi\rangle_0 = |\psi\rangle \otimes |0\rangle$. The first state vector can be interpreted as a qubit system in the state $|\psi\rangle$, and the second as an *ancilla* in the state $|0\rangle$. But note that the state $|\psi\rangle_0 = (\alpha, 0, \beta, 0)^T$ is different from the initial state shown in Fig. 1, given by $|\psi\rangle_{\text{in}} = (0, \alpha, \beta, 0)^T$. The input state $|\psi\rangle_{\text{in}}$ can be written in terms of the state $|\psi\rangle_0$, with no modifications in the circuit nor any relabeling, by using the transformation described by $\hat{M}$, defined by the following relation:

$$\begin{bmatrix} 0 \\ \alpha \\ \beta \\ 0 \end{bmatrix} = \hat{M} \begin{bmatrix} \alpha \\ 0 \\ \beta \\ 0 \end{bmatrix} \quad \Rightarrow \quad \hat{M} = \begin{bmatrix} 0 & 1 & 0 & 0 \\ 1 & 0 & 0 & 0 \\ 0 & 0 & 1 & 0 \\ 0 & 0 & 0 & 1 \end{bmatrix}. \tag{10}$$

It is worth noting that the transformation $\hat{M}$ is not implemented in practice. It is only a mathematical transformation. Thus, as our proposal supposes the input state as being $|\psi\rangle_{\text{in}}$ and the theoretical calculation is made based on the initial state $|\psi\rangle_0$, we have

$$\hat{U}'|\psi\rangle_{\text{in}} = \hat{T}_3\hat{T}_2\hat{T}_1\hat{M}|\psi\rangle_0. \tag{11}$$

Therefore, the operator that effectively would act on the state $|\psi\rangle_0$ is given by

$$\hat{U}_{\text{qubit}} = \hat{T}_3\hat{T}_2\hat{T}_1\hat{M}. \tag{12}$$

The operator defined in Eq. (12) is used in the process of determination of the circuit parameters, as shown in Appendix A.

The next task is to find the parameters r_j, t_j, and ϕ_j that compose $\hat{U}_{\text{qubit}}$ to complete the circuit description. We start by examining the set of probability operators $\hat{\Pi}_{ml}$ acting on the system-ancilla Hilbert space. Such operators can be understood as the POVM elements associated with the detection of the photon at each circuit output. The action results of these POVM elements correspond to the projections over the states of the set $\{|ml\rangle\}$, with $m, l = 0, 1$, and each circuit output corresponds to one of the states $|ml\rangle$, i.e., $|00\rangle$, $|01\rangle$, $|10\rangle$, or $|11\rangle$. Here the states $|m\rangle$ and $|l\rangle$ form a basis on each of the subspaces: system and ancilla, respectively. The probability of detecting a photon, initially in the state described by the density operator $\hat{\rho}$, in one given output of the interferometer, is given by

$$P_{ml} = \text{Tr}[(\hat{\rho} \otimes |0\rangle\langle 0|)\hat{\Pi}_{ml}], \tag{13}$$

where $|0\rangle$ is the ancilla state. This expression can also be written in terms of a POVM acting only in the subspace of the input qubit

$$P_{ml} = \text{Tr}[\hat{\rho}\hat{E}_{ml}], \tag{14}$$

where we can define the local POVM elements $\hat{E}_{ml}$ as

$$\hat{E}_{ml} = \text{Tr}_2[(\hat{\mathbb{I}} \otimes |0\rangle\langle 0|)\hat{U}^{\dagger}_{\text{qubit}}|ml\rangle\langle ml|\hat{U}_{\text{qubit}}] \tag{15}$$

and the matrix elements of $\hat{E}_{ml}$ will be given by

$$\langle p|\hat{E}_{ml}|q\rangle = \langle p0|\hat{U}^{\dagger}_{\text{qubit}}|ml\rangle\langle ml|\hat{U}_{\text{qubit}}|q0\rangle. \tag{16}$$

Each state $|ml\rangle$, in binary notation, corresponds to one outcome shown in Fig. 1, which allows us to make the exchange $\hat{E}_{ml} \to \hat{E}_k$, with k being the number that identifies each output. Based on this, the operators $\hat{E}_k$ in Eq. (15) will be identified as the POVM element presented in Eq. (2). From these relations, it is possible to determine the suitable circuit parameters. As shown in Appendix A, the parameters necessary for implementing the minimal tomography, in this case, are

$$r_1 = 1/3, \quad t_1 = 2/3, \quad \phi_1 = \pi/2, \tag{17a}$$
$$r_2 = 1/3, \quad t_2 = 2/3, \quad \phi_2 = 0, \tag{17b}$$
$$r_3 = 0, \quad t_3 = 1, \quad \phi_3 = 0, \tag{17c}$$
$$r_4 = 1/2, \quad t_4 = 1/2, \quad \phi_4 = 0, \tag{17d}$$
$$r_5 = 1/2, \quad t_5 = 1/2, \quad \phi_5 = 0. \tag{17e}$$

By manufacturing a photonic circuit (Fig. 1) with the parameters presented in Eqs. (17), we obtain a specific interferometer with five beam splitters and one phase shifter. This circuit implements POVM by doing unitary transformations and projective measurements in an extended Hilbert space with less optical elements and a smaller optical depth than other existing general unitary operations circuits already proposed in the literature [63–65]. Another conclusion that arises from this result, is that the effect of the beam splitter that composes $\hat{T}_2$ solely exchanges the photon beam carried by the second and third paths, as seen in Eq. (17c). Except by this exchange, the BS's that act nontrivially operate only between the first and second, and the third and fourth, separately. This structure will inspire the design of circuits for general qudit states.

IV. MINIMUM QUANTUM STATE TOMOGRAPHY FOR QUTRITS

For the qutrit, we approached the circuit's design in a different manner. The strategy to find a circuit that performs the qubit's tomography starts with Eq. (12), which leads to the solution of a 4×4 matrix equation for finding the BS specifications. Applying the same procedure in the qutrit case would result in the solution of a 9×9 matrix equation. Alternatively, we faced this problem by analyzing the POVM operators and the desired outcomes for the qutrit tomography, being able to reduce the problem to the search of a 3×3 matrix equation solution. The qutrit tomography is realized via equidistant states [21,54].

The SIC-POVM elements for the qutrit case are of the form

$$\hat{E}_{ml} = \tfrac{1}{3}|\psi_{ml}\rangle\langle\psi_{ml}|, \tag{18}$$

with $m, l = 0, 1, 2$ and [54]

$$|\psi_{00}\rangle = \mu|0\rangle + \eta|2\rangle, \tag{19a}$$
$$|\psi_{01}\rangle = \kappa|0\rangle + \kappa|2\rangle, \tag{19b}$$
$$|\psi_{02}\rangle = \eta|0\rangle + \mu|2\rangle, \tag{19c}$$
$$|\psi_{10}\rangle = \eta|0\rangle + \mu|1\rangle, \tag{19d}$$
$$|\psi_{11}\rangle = \kappa|0\rangle + \kappa|1\rangle, \tag{19e}$$
$$|\psi_{12}\rangle = \mu|0\rangle + \eta|1\rangle, \tag{19f}$$
$$|\psi_{20}\rangle = \eta|1\rangle + \mu|2\rangle, \tag{19g}$$
$$|\psi_{21}\rangle = \kappa|1\rangle + \kappa|2\rangle, \tag{19h}$$
$$|\psi_{22}\rangle = \mu|1\rangle + \eta|2\rangle, \tag{19i}$$

where $\kappa = 1/\sqrt{2}$, $\mu = e^{2\pi i/3}/\sqrt{2}$, and $\eta = e^{-2\pi i/3}/\sqrt{2}$, such that $\kappa + \mu + \eta = 0$, ensuring that $\sum_{ml} \hat{E}_{ml} = \mathbb{1}$. Keeping in mind Eq. (16), we use the fact that the POVM elements are of the form of Eq. (18) to define a^p_{ml} as the expansion coefficients of $|\psi_{ml}\rangle$ as

$$\frac{1}{\sqrt{3}}|\psi_{ml}\rangle = a^0_{ml}|0\rangle + a^1_{ml}|1\rangle + a^2_{ml}|2\rangle, \tag{20}$$

where $\langle p|\hat{E}_{ml}|q\rangle = (a^p_{ml})^* a^q_{ml}$, with $p, q = 0, 1, 2$. By substituting Eq. (20) into Eq. (18) and comparing $\hat{E}_{ml}$ with Eq. (16), we arrive at an expression for the matrix elements of $\hat{U}$ that allow us to implement the desired POVM elements in the extended Hilbert space of dimension 9

$$\langle ml|\hat{U}|q0\rangle = a^q_{ml}. \tag{21}$$

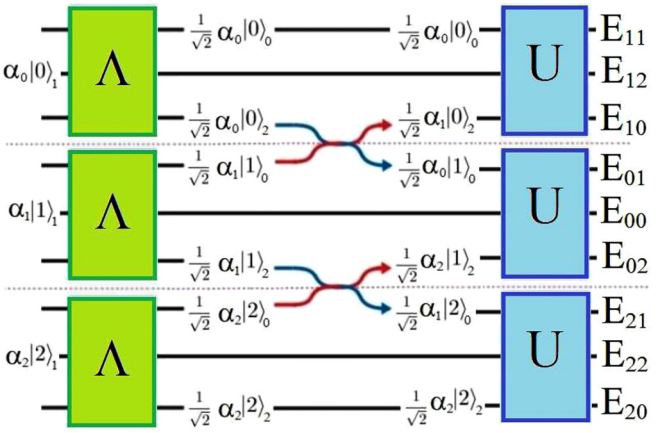

FIG. 2. Schematic drawing showing the quantum operations of the proposed photonic circuit for quantum tomography of qutrits. The pink dotted lines separate the three sectors of the circuit that can be analyzed separately. The waveguides are represented by the black lines and labeled by the vectors $|i\rangle_j$, where $i, j = 0, 1, 2$. The state vectors $\alpha_i|i\rangle_1$ indicate the waveguides where a possible $(\alpha_0, \alpha_1, \alpha_2)^T$ input qutrit path state is coupled to the circuit. The $\hat{\Lambda}$ operation is responsible for diffusing the initial state to the first and third path in each sector. The red and blue arrows portray the permutations between the third and fourth paths and between the sixth and seventh ones, respectively. This permutation, performed by $1:0$ BS, exchanges the coefficients of some base vectors. Finally, these paths are connected to the last circuit piece, described by a 3×3 $\hat{U}$ matrix, to resume the tomographic implementation. Analogous descriptions can be done for the other two sectors. A detector count in one of the nine circuit outputs is proportional to the implementation probability of a POVM element $\hat{E}_{ij}$ $(i, j = 0, 1, 2)$.

Inspired by the solution for the tomography of qubits, we conceive an interferometer that is formed by three sectors, shown in Fig. 2, separated by the pink dotted line. Due to the symmetry in the POVM, it is convenient to perform the tomography measurements, such that, in the kth sector, the three outcomes result from the application of only $\hat{E}_{kl}$ $(l = 0, 1, 2)$, already defined in Eq. (18). Our goal is that the photon count in the detector coupled to one of the three exits of the zeroth, first, and second sector is proportional to the probability of implementing the POVM elements $\hat{E}_{0l}$, $\hat{E}_{1l}$, or $\hat{E}_{2l}$, respectively.

The prepared photonic path state is such that the photon can enter in one of the nine input ports of the interferometer, as shown in Fig. 2. A photon in a qutrit path state represented by the $|0\rangle$, $|1\rangle$, and $|2\rangle$ base vectors can enter in the second or in the fifth or in the eighth input circuit ports. Since the photonic circuit has nine input ports, it is clear that the Hilbert space for the photonic path states increases from $N = 3$ to $N = 9$. We label the path states in the $N = 9$ extended Hilbert space as $|i\rangle_j$, where $i, j = 0, 1, 2$. The nine photonic paths, from top to bottom, are labeled as $|0\rangle_0$, $|0\rangle_1$, $|0\rangle_2$, $|1\rangle_0$, $|1\rangle_1$, $|1\rangle_2$, $|2\rangle_0$, $|2\rangle_1$, and $|2\rangle_2$. Figure 2 shows the quantum operations schematically in the extended Hilbert space.

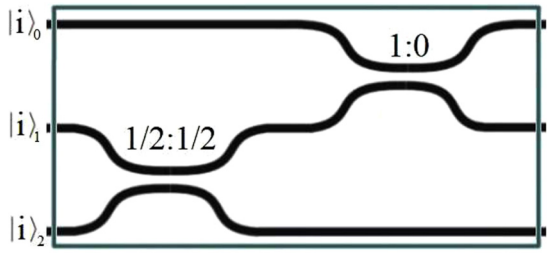

FIG. 3. Circuit representation of the $\hat{\Lambda}$ operation for the implementation of the qutrit tomography. We have a $1/2:1/2$ BS that splits the input mode in path 2 in two output modes in paths 2 and 3 (labeled as $|i\rangle_1$ and $|i\rangle_2$, respectively). A $1:0$ BS between paths 1 and 2 switches these paths.

Let us suppose we have a normalized input state $|\psi\rangle = \sum_{i=0}^{2} \alpha_i |i\rangle_1$. After the first operation, represented by the green rectangles, the photon path state becomes $|\psi'\rangle = \sum_{i=0}^{2} \alpha_i (|i\rangle_0 + |i\rangle_2)/\sqrt{2}$. The second transformation in Fig. 2 switches some of the coefficients in $|\psi'\rangle$ to generate the state $|\psi''\rangle = \sum_{i=0}^{2} (\beta_i |i\rangle_0 + \gamma_i |i\rangle_2)/\sqrt{2}$, where $\beta_0 = \beta_1 = \alpha_0$, $\beta_2 = \gamma_0 = \alpha_1$, and $\gamma_1 = \gamma_2 = \alpha_2$. The states $|\psi\rangle$ and $|\psi''\rangle$ can be represented by vectors such that the first and second state transformations in Fig. 2 produces

$$\begin{bmatrix} 0 \\ \alpha_0 \\ 0 \\ 0 \\ \alpha_1 \\ 0 \\ 0 \\ \alpha_2 \\ 0 \end{bmatrix} \longmapsto \frac{1}{\sqrt{2}} \begin{bmatrix} \alpha_0 \\ 0 \\ \alpha_1 \\ \alpha_0 \\ 0 \\ \alpha_2 \\ \alpha_1 \\ 0 \\ \alpha_2 \end{bmatrix}. \tag{22}$$

Notice that the circuit design is such that, in the first, second, and third sectors, we create state superpositions of the original qutrit base states $\{|0\rangle, |1\rangle\}$, $\{|0\rangle, |2\rangle\}$, and $\{|1\rangle, |2\rangle\}$, respectively. The arrangement of beam splitters which implements what is outlined by the green rectangles in Fig. 2 is shown in Fig. 3. The optical couplers (BS) that carry the quantum operation described in Fig. 3 are $1/2:1/2$ BS ($t = 0.5$ and $r = 0.5$) and $1:0$ BS ($t = 1$ and $r = 0$). The second transformation shown in Fig. 2, the permutations between third and fourth paths and sixth and seventh paths, is performed by $1:0$ BSs.

The last part of Fig. 2 shows the applications of unitary operations $\hat{U}$ in the first, second, and third sectors. Notice that the $\hat{U}$ operations only apply to the vector states of their respective sectors. Therefore, the quantum operation described by a 9×9 matrix in the extended Hilbert space of nine dimensions is composed by three 3×3 $\hat{U}$ matrices forming three blocks matrices with all the other elements of the 9×9 matrix equal to zero, i.e.,

$$\hat{O} = \begin{bmatrix} \hat{U} & 0 & 0 \\ 0 & \hat{U} & 0 \\ 0 & 0 & \hat{U} \end{bmatrix}. \tag{23}$$

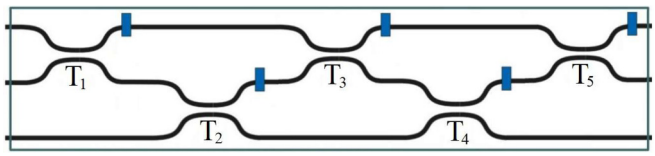

FIG. 4. Circuit representation of the $\hat{U}$ matrix for the implementation of the qutrit tomography. The blue rectangles are phase shifters.

The circuit scheme for $\hat{U}$ appears in detail in Fig. 4. Hence, we must establish the coefficients r_j, t_j, and the phases ϕ_j. In order to achieve this, we are going to obtain the matrix from the inputs and outputs vectors available. The desired effect of the operations $\hat{E}_{0l}$, $\hat{E}_{1l}$, and $\hat{E}_{2l}$ in the first, second, and third sectors of the circuit, respectively, leads us to

$$\hat{U} \begin{bmatrix} \alpha_i/\sqrt{2} \\ 0 \\ \alpha_j/\sqrt{2} \end{bmatrix} = \frac{1}{\sqrt{6}} \begin{bmatrix} \alpha_i + \alpha_j \\ \alpha_i e^{2i\pi/3} + \alpha_j e^{-2i\pi/3} \\ \alpha_i e^{-2i\pi/3} + \alpha_j e^{2i\pi/3} \end{bmatrix}, \tag{24}$$

with $i = 0, 1$, $j = 1, 2$, and $i < j$. The unitary $\hat{U}$ that satisfies Eq. (24) is

$$\hat{U} = \frac{1}{\sqrt{3}} \begin{bmatrix} 1 & 1 & 1 \\ e^{2i\pi/3} & 1 & e^{-2i\pi/3} \\ e^{-2i\pi/3} & 1 & e^{2i\pi/3} \end{bmatrix}, \tag{25}$$

which corresponds to the circuit in Fig. 4. We managed therefore to reduce the problem from a 9×9 matrix equation to a problem of finding coefficients for a 3×3 matrices. Performing this calculation (more details in Appendix B), we obtain the values of the coefficients and phases:

$$r_1 = 1, \quad t_1 = 0, \quad \phi_1 = -2\pi/3, \tag{26a}$$
$$r_2 = 0, \quad t_2 = 1, \quad \phi_2 = -\pi/3, \tag{26b}$$
$$r_3 = 1/2, \quad t_3 = 1/2, \quad \phi_3 = -\pi/2, \tag{26c}$$
$$r_4 = 1/3, \quad t_4 = 2/3, \quad \phi_4 = 0, \tag{26d}$$
$$r_5 = 1/2, \quad t_5 = 1/2, \quad \phi_5 = \pi. \tag{26e}$$

The results presented in Eqs. (26) show that the first beam splitter of the scheme of Fig. 4 can be discarded, since there is no transmittance. The phase shifter ϕ_5 can also be discarded, since it is at the end of the circuit and does not interfere in the photon counting. We conclude that the interferometer that implements the quantum path state tomography in the one-qutrit state is formed by 20 beam splitters and nine phase shifters. As in the one-qubit case, our proposal for one-qutrit systems has less optical elements and a smaller optical depth than other existing proposals in the literature [63–65].

We also summarize in Table I the number of optical elements necessary for the implementation of each proposal of photonic circuits for the quantum tomography task. It is worth emphasizing that Reck's and Clements's proposals use Mach-Zehnder interferometers as building blocks of the circuits, while our proposal uses single beam splitters.

TABLE I. Number of optical elements required for the implementation of minimum quantum path state tomography in photonic circuits according to our proposal and other proposals already known in the literature [63–65].

	Reck's proposal	Clements's proposal	Tabia's proposal	Our proposal
Qubit	12	12	7	6
Qutrit	72	72	44	29

V. GENERALIZATION FOR *N* DIMENSIONS

In the previous section we use the results of Paiva-Sánchez [54] about equidistant states to build the SIC-POVM elements that implement a quantum state tomography of path photonic qutrits. One remarkable feature of this approach is that it is not limited to the dimension of the input state. The relation for equidistant states suitable for the tomography of an N-dimensional quantum system is [54]

$$|\psi_l\rangle = \frac{1}{\sqrt{N-1}} \sum_{\substack{k=0 \\ k\neq 1}}^{N-1} e^{2i\pi l(k-1)/N}|k\rangle, \tag{27}$$

where $l = 0, 1, \ldots, N-1$. From Eq. (27) we can obtain N operators of the N^2 required for the quantum state tomography experiment. The other operators are obtained from states generated by the application of the operator $\hat{X}$ in $|\psi_l\rangle$ shown in Eq. (27), defined as

$$\hat{X}|k\rangle = |k \oplus 1\rangle. \tag{28}$$

This operator $\hat{X}$ acts on a state $|k\rangle$ performing an addition modulo N. Thus, all equidistant states used in the construction of the POVM elements can be organized in sets $B_m(\psi)$, with $m = 0, 1, \ldots, N-1$, defined as

$$B_m(\psi) = \{|\psi_{ml}\rangle = \hat{X}^m|\psi_l\rangle\} \tag{29}$$

and these POVM elements are obtained through the relation

$$\hat{E}_{ml} = \frac{1}{N}|\psi_{ml}\rangle\langle\psi_{ml}|. \tag{30}$$

As an example, we will define the base states for quantum state tomography of ququarts, that is, qudits with $N = 4$. They are

$$|\psi_{00}\rangle = \frac{1}{\sqrt{3}}(|0\rangle + |2\rangle + |3\rangle), \tag{31a}$$

$$|\psi_{01}\rangle = \frac{1}{\sqrt{3}}(-i|0\rangle + i|2\rangle - |3\rangle), \tag{31b}$$

$$|\psi_{02}\rangle = \frac{1}{\sqrt{3}}(-|0\rangle - |2\rangle + |3\rangle), \tag{31c}$$

$$|\psi_{03}\rangle = \frac{1}{\sqrt{3}}(i|0\rangle - i|2\rangle - |3\rangle). \tag{31d}$$

The other states ($|\psi_{1l}\rangle$, $|\psi_{2l}\rangle$, and $|\psi_{3l}\rangle$, with $l = 0, 1, 2, 3$) come from the application of the operator $\hat{X}$ one, two, or three times.

The determination of the circuit design for the general case is made in the same way as it was done in Sec. IV, not applicable for the qubit case. The N^2 paths are divided into N sectors with N paths each. Here the three-dimensional (3D) conception of circuits facilitates the generalization task [68–70]. The assumption of a 3D waveguide writing technique becomes necessary because we have to create path states superposition between states of different sectors. For example, it is necessary to create superposition between the states of the first and the last sector in a SIC-POVM tomographic proposal. In a planar circuit, the optical depth would increase, as long as these states are connected, by a quadratic function in N. In the 3D waveguide writing technique, these states will be connected by $N-1$ beam splitters, that is, the optical depth is now a linear function in N.

In the three-dimensional circuit scheme, the paths can be organized in N parallel vertical sectors, with N paths in the vertical direction each, forming a square array of waveguides. By choosing the paths for entrance of the photons belonging to the same line, i.e., path i_0 in each sector j, we have as initial state

$$|\psi\rangle_j^{(0)} = \sum_{j=0}^{N-1} \alpha_j|i_0 j\rangle, \tag{32}$$

where $|i_0 j\rangle$ means path state in line i_0 and sector j. Our proposal consists of conceiving the circuit as a sequence of three unitary operations. The first one operates separately in each vertical sector j performing the transformation

$$\alpha_j|i_0 j\rangle \quad \longmapsto \quad \frac{\alpha_j}{\sqrt{N-1}} \sum_{i=0}^{N-2} |ij\rangle, \tag{33}$$

i.e., each component of the initial state $\alpha_j|i_0 j\rangle$ is decomposed into $N-1$ components $\alpha_j|ij\rangle$, that will occupy $N-1$ paths of the vertical sector j, leaving, also by choice, the last path empty.

The second operation realized by the circuit is a permutation betweens vertical sectors. Except the last layer that did not receive one of the $N-1$ components at the end of the first operation, in all other layers the operation performed is an addiction modulo N as follows:

$$\hat{\Gamma}|ij\rangle = |i\rangle|j \oplus i\rangle, \tag{34}$$

where $i = 0, 1, \ldots, N-2$ is the paths label. At the end of this second operation, we will have in each vertical sector j the state

$$|\psi\rangle_j^{(2)} = \frac{1}{\sqrt{N-1}} \sum_{i=0}^{N-2} \alpha_{j-i}|ij\rangle, \tag{35}$$

where the operations with subindexes are carried out modulo N. The third operation that our proposed circuit performs is analogous to Eq. (25). Its transforms the state $|\psi\rangle_j^{(2)}$ [Eq. (35)] in a final state where the square module of its expansion coefficients are equal to the probabilities that implement all POVM elements in the qudit Hilbert space. By possession

of these probabilities, we reconstruct the initial state density matrix [54].

If the possibility of usage of a three-dimensional array is at hand, our circuit becomes considerably more efficient than one derived directly from [64] or [65]. As the minimal state tomography uses at least N^2 outputs, a general circuit would have a complexity of $O(N^4)$ beam splitters. In our realization, the procedure is divided into three parts, each acting in parallel over a maximum N paths. This guarantees a complexity of $O(N^3)$. Moreover, each part may simplify separately, since they act differently, allowing an increase of efficiency through the detailed analysis of each part. The modular property of the circuit is the main feature of our proposed implementation of the circuit for minimal state tomography.

There is a particularity in the even-dimension case, reported in Ref. [54]. It is shown that the method exposed in this paper cannot determine the imaginary part of some elements of the system's density matrix $\hat{\rho}$. For that, one more step is needed, the application of the following operator:

$$\hat{\Xi} = \sum_{k=0}^{N/2-1} |k\rangle\langle k| + i \sum_{N/2}^{N-1} |k\rangle\langle k|, \tag{36}$$

which generates a new density matrix $\hat{\rho}' = \hat{\Xi}\hat{\rho}\hat{\Xi}^\dagger$. The advantage about this strategy is that the imaginary parts, impossible to be determined, are exchanged with the real parts of the same matrix elements, being now possible to be obtained. Thus, to reconstruct the initial density matrix of even-dimensional systems, it is necessary to realize the quantum state tomography in $\hat{\rho}$ and $\hat{\rho}'$, increasing from N^2 to $3N^2/2$ the number of measurements.

VI. CONCLUSION

In this paper we were able to determine the design of integrated photonic circuits that perform quantum path state tomography for qubits and qutrits. In these schemes, a POVM is implemented by doing an application of Naimark's theorem by extending the qudit Hilbet space, performing unitary transformations and projective measurements in this extended space. The parameters of the optical interferometer elements (beam splitters and phase shifters) were accurately calculated by using methods already described in the literature. Only three different types of beam splitters appeared on the proposed circuits, which may facilitate their manufacture. Our designs require less optical components than alternative general unitary transformations circuits and a smaller optical depth when compared with the optical depth of the circuits discussed in [64,65]. A general recipe also was presented for determining the circuit to be used for dimensions higher than three. In all cases, our interferometers are more compact than those already exposed in other works.

ACKNOWLEDGMENTS

This research was supported by the Brazilian agencies CNPq - Conselho Nacional de Desenvolvimento Científico e Tecnológico, Capes - Coordenação de Aperfeiçoamento de Pessoal de Nível Superior, Fapemig - Fundação de Amparo à Pesquisa do Estado de Minas Gerais, and INCT-IQ - Instituto Nacional de Ciência e Tecnologia de Informação Quântica.

APPENDIX A: CALCULATIONS FOR THE QUBIT PHOTONIC CIRCUIT

In Sec. II are defined the POVM elements that realize a full quantum state tomography in one-qubit systems, namely

$$\hat{E}_1 = \frac{1}{2}\begin{bmatrix} 2/3 & -i\sqrt{2}/3 \\ i\sqrt{2}/3 & 1/3 \end{bmatrix}, \tag{A1}$$

$$\hat{E}_2 = \frac{1}{2}\begin{bmatrix} 2/3 & i\sqrt{2}/3 \\ -i\sqrt{2}/3 & 1/3 \end{bmatrix}, \tag{A2}$$

$$\hat{E}_3 = \frac{1}{2}\begin{bmatrix} 1/3 & -\sqrt{2}/3 \\ -\sqrt{2}/3 & 2/3 \end{bmatrix}, \tag{A3}$$

$$\hat{E}_4 = \frac{1}{2}\begin{bmatrix} 1/3 & \sqrt{2}/3 \\ \sqrt{2}/3 & 2/3 \end{bmatrix}. \tag{A4}$$

On the other hand, the POVM elements written in terms of the parameters of the photonic circuit that we aim to determine are expressed in Eq. (15), where $|m\rangle$ and $|l\rangle$ are the state vectors of the subspace basis, principal system, and ancilla, respectively. Instead of labeling the outcomes in terms of the binary base $|ml\rangle$, we choose to label the output states in terms of the path number of the circuit, where we write $\hat{\rho}_k = |k\rangle\langle k|$. Therefore, we make the identification:

$$\begin{aligned} m = 0, l = 0 \quad &\rightarrow \quad k = 1, \\ m = 0, l = 1 \quad &\rightarrow \quad k = 2, \\ m = 1, l = 0 \quad &\rightarrow \quad k = 3, \\ m = 1, l = 1 \quad &\rightarrow \quad k = 4. \end{aligned} \tag{A5}$$

Moreover, these operators are simplified if we define the beam splitter in $\hat{T}_2$ as a $1:0$ BS, so that $r_3 = 0$ and $t_3 = 1$. With this, the operators are reduced to

$$\hat{E}_1 = \begin{bmatrix} r_4 t_1 & e^{-i\theta}\sqrt{r_2 r_4 t_1 t_4} \\ e^{i\theta}\sqrt{r_2 r_4 t_1 t_4} & r_2 t_4 \end{bmatrix}, \tag{A6}$$

$$\hat{E}_2 = \begin{bmatrix} t_1 t_4 & -e^{-i\theta}\sqrt{r_2 r_4 t_1 t_4} \\ -e^{i\theta}\sqrt{r_2 r_4 t_1 t_4} & r_2 r_4 \end{bmatrix}, \tag{A7}$$

$$\hat{E}_3 = \begin{bmatrix} r_1 r_5 & -\sqrt{r_1 r_5 t_2 t_5} \\ -\sqrt{r_1 r_5 t_2 t_5} & t_2 t_5 \end{bmatrix}, \tag{A8}$$

$$\hat{E}_4 = \begin{bmatrix} r_1 t_5 & \sqrt{r_1 r_5 t_2 t_5} \\ \sqrt{r_1 r_5 t_2 t_5} & r_5 t_2 \end{bmatrix}, \tag{A9}$$

where $\theta = \phi_1 - \phi_2 - \phi_3$. The absence of the phases ϕ_4 and ϕ_5 in the operators $\hat{E}_k$ allows us to choose

$$\phi_4 = 0, \quad \phi_5 = 0. \tag{A10}$$

When comparing $\hat{E}_1$ [Eq. (A1)] with $\hat{E}_1$ [Eq. (A6)] and $\hat{E}_2$ [Eq. (A2)] with $\hat{E}_2$ [Eq. (A7)], it is concluded that

$$r_4 = t_4 \quad \Rightarrow \quad r_4 = 1/2, \quad t_4 = 1/2. \tag{A11}$$

Similarly, when comparing $\hat{E}_3$ [Eq. (A3)] with $\hat{E}_3$ [Eq. (A8)] and $\hat{E}_4$ [Eq. (A4)] with $\hat{E}_4$ [Eq. (A9)], it is

concluded that

$$r_5 = t_5 \quad \Rightarrow \quad r_5 = 1/2, \quad t_5 = 1/2. \tag{A12}$$

Therefore, the operators acquire simpler forms:

$$\hat{E}_1 = \frac{1}{2}\begin{bmatrix} t_1 & e^{-i\theta}\sqrt{r_2 t_1} \\ e^{i\theta}\sqrt{r_2 t_1} & r_2 \end{bmatrix}, \tag{A13}$$

$$\hat{E}_2 = \frac{1}{2}\begin{bmatrix} t_1 & -e^{-i\theta}\sqrt{r_2 t_1} \\ -e^{i\theta}\sqrt{r_2 t_1} & r_2 \end{bmatrix}, \tag{A14}$$

$$\hat{E}_3 = \frac{1}{2}\begin{bmatrix} r_1 & -\sqrt{r_1 t_2} \\ -\sqrt{r_1 t_2} & t_2 \end{bmatrix}, \tag{A15}$$

$$\hat{E}_4 = \frac{1}{2}\begin{bmatrix} r_1 & \sqrt{r_1 t_2} \\ \sqrt{r_1 t_2} & t_2 \end{bmatrix}. \tag{A16}$$

Making the same comparisons explained above, we obtain the last parameters of the circuit:

$$\begin{matrix} r_1 = 1/3, & t_1 = 2/3, \\ r_2 = 1/3, & t_2 = 2/3, \end{matrix} \quad \theta = \pi/2. \tag{A17}$$

APPENDIX B: CALCULATIONS FOR THE $\hat{U}$ MATRIX OF THE QUTRIT PHOTONIC CIRCUIT

We are interested to find the parameters necessary for carrying the operator $\hat{U}$ shown in Eq. (25). The circuit representation of the $\hat{U}$ matrix is shown in Fig. 4. The operations that make up this circuit are

$$\hat{T}_a = \begin{bmatrix} e^{i\phi_a}\sqrt{r_a} & e^{i\phi_a}\sqrt{t_a} & 0 \\ \sqrt{t_a} & -\sqrt{r_a} & 0 \\ 0 & 0 & 1 \end{bmatrix}, \tag{B1}$$

$$\hat{T}_b = \begin{bmatrix} 1 & 0 & 0 \\ 0 & e^{i\phi_b}\sqrt{r_b} & e^{i\phi_b}\sqrt{t_b} \\ 0 & \sqrt{t_b} & -\sqrt{r_b} \end{bmatrix}, \tag{B2}$$

where $a = 1, 3, 5$ and $b = 2, 4$. The entire circuit is represented by the matrix

$$\hat{U}_{\text{qutrit}} = \hat{T}_5\hat{T}_4\hat{T}_3\hat{T}_2\hat{T}_1. \tag{B3}$$

Analogous to the qubit case, it is possible to simplify the matrix $\hat{U}_{\text{qutrit}}$ by defining $r_1 = 1$, $t_1 = 0$, $r_2 = 0$, and $t_2 = 1$. This reduces the matrix elements to the following quantities:

$$\begin{aligned}
\langle 0|\hat{U}_{\text{qutrit}}|0\rangle &= e^{i(\phi_1+\phi_5)}(e^{i\phi_3}\sqrt{r_3 r_5} + e^{i\phi_4}\sqrt{r_4 t_3 t_5}),\\
\langle 0|\hat{U}_{\text{qutrit}}|1\rangle &= -e^{i(\phi_4+\phi_5)}\sqrt{t_4 t_5},\\
\langle 0|\hat{U}_{\text{qutrit}}|2\rangle &= e^{i(\phi_2+\phi_5)}(e^{i\phi_3}\sqrt{r_5 t_3} - e^{i\phi_4}\sqrt{r_3 r_4 t_5}),\\
\langle 1|\hat{U}_{\text{qutrit}}|0\rangle &= e^{i\phi_1}(-e^{i\phi_4}\sqrt{r_4 r_5 t_3} + e^{i\phi_3}\sqrt{r_3 t_5}),\\
\langle 1|\hat{U}_{\text{qutrit}}|1\rangle &= -e^{i\phi_4}\sqrt{r_5 t_4},\\
\langle 1|\hat{U}_{\text{qutrit}}|2\rangle &= e^{i\phi_2}(e^{i\phi_4}\sqrt{r_3 r_4 r_5} + e^{i\phi_3}\sqrt{t_3 t_5}),\\
\langle 2|\hat{U}_{\text{qutrit}}|0\rangle &= e^{i\phi_1}\sqrt{t_3 t_4},\\
\langle 2|\hat{U}_{\text{qutrit}}|1\rangle &= \sqrt{r_4},\\
\langle 2|\hat{U}_{\text{qutrit}}|2\rangle &= -e^{i\phi_2}\sqrt{r_3 t_4}.
\end{aligned}$$

A first comparison between the elements of the matrix $\hat{U}_{\text{qutrit}}$ and those of the matrix $\hat{U}$ in Eq. (25) allows us to determine the following parameters:

$$\begin{matrix} r_3 = 1/2, & t_3 = 1/2, & \phi_1 = -2\pi/3, \\ r_4 = 1/3, & t_4 = 2/3, & \phi_2 = -\pi/3. \end{matrix} \tag{B4}$$

With the parameters shown in Eq. (B4), the matrix elements $\langle 2|\hat{U}_{\text{qutrit}}|j\rangle$ $(j = 0, 1, 2)$, are determined completely. The parameters ϕ_j $(j = 3, 4, 5)$, r_5, and t_5 of the remaining elements are still not determined, as shown below:

$$\begin{aligned}
\langle 0|\hat{U}_{\text{qutrit}}|0\rangle &= e^{i(\phi_5-2\pi/3)}(e^{i\phi_3}\sqrt{r_5/2} + e^{i\phi_4}\sqrt{t_5/6}),\\
\langle 0|\hat{U}_{\text{qutrit}}|1\rangle &= -e^{i(\phi_4+\phi_5)}\sqrt{2t_5/3},\\
\langle 0|\hat{U}_{\text{qutrit}}|2\rangle &= e^{i(\phi_5-\pi/3)}(e^{i\phi_3}\sqrt{r_5/2} - e^{i\phi_4}\sqrt{t_5/6}),\\
\langle 1|\hat{U}_{\text{qutrit}}|0\rangle &= e^{-2i\pi/3}(-e^{i\phi_4}\sqrt{r_5/6} + e^{i\phi_3}\sqrt{t_5/2}),\\
\langle 1|\hat{U}_{\text{qutrit}}|1\rangle &= -e^{i\phi_4}\sqrt{2r_5/3},\\
\langle 1|\hat{U}_{\text{qutrit}}|2\rangle &= e^{-i\pi/3}(e^{i\phi_4}\sqrt{r_5/6} + e^{i\phi_3}\sqrt{t_5/2}).
\end{aligned}$$

When comparing again the elements $\langle i|\hat{U}_{\text{qutrit}}|j\rangle$ $(i = 0, 1,$ $j = 0, 1, 2)$ and the respective elements of the $\hat{U}$ matrix in Eq. (25), we are able to determine the remaining parameters

$$\begin{matrix} r_5 = 1/2, & t_5 = 1/2, \\ \phi_3 = 1/3, & \phi_4 = 2/3, & \phi_5 = -\pi/3. \end{matrix} \tag{B5}$$

Thus, we obtained $\hat{U}_{\text{qutrit}} = \hat{U}$ as we wanted.

[1] P. Rungta, W. J. Munro, K. Nemoto, P. Deuar, G. J. Milburn, and C. M. Caves, Qudit entanglement, in *Directions in Quantum Optics* (Springer, Berlin, 2001), pp. 149–164.

[2] R. T. Thew, A. Acin, H. Zbinden, and N. Gisin, Bell-Type Test of Energy-Time Entangled Qutrits, Phys. Rev. Lett. **93**, 010503 (2004).

[3] R. T. Thew, K. Nemoto, A. G. White, and W. J. Munro, Qudit quantum-state tomography, Phys. Rev. A **66**, 012303 (2002).

[4] L. Neves, G. Lima, J. G. A. Gómez, C. H. Monken, C. Saavedra, and S. Pádua, Generation of Entangled States of Qudits Using Twin Photons, Phys. Rev. Lett. **94**, 100501 (2005).

[5] E. V. Moreva, G. A. Maslennikov, S. S. Straupe, and S. P. Kulik, Realization of Four-Level Qudits Using Biphotons, Phys. Rev. Lett. **97**, 023602 (2006).

[6] Y. Li, K. Zhang, and K. Peng, Generation of qudits and entangled qudits, Phys. Rev. A **77**, 015802 (2008).

[7] F. Steinlechner, S. Ecker, M. Fink, B. Liu, J. Bavaresco, M. Huber, T. Scheidl, and R. Ursin, Distribution of high-dimensional entanglement via an intra-city free-space link, Nat. Commun. **8**, 15971 (2017).

[8] M. Hendrych, R. Gallego, M. Mičuda, N. Brunner, A. Acín, and J. P. Torres, Experimental estimation of the dimension

of classical and quantum systems, Nat. Phys. **8**, 588 (2012).

[9] M. Kues, C. Reimer, P. Roztocki, L. R. Cortés, S. Sciara, B. Wetzel, Y. Zhang, A. Cino, S. T. Chu, B. E. Little *et al.*, On-chip generation of high-dimensional entangled quantum states and their coherent control, Nature (London) **546**, 622 (2017).

[10] J. Wang, S. Paesani, Y. Ding, R. Santagati, P. Skrzypczyk, A. Salavrakos, J. Tura, R. Augusiak, L. Mančinska, D. Bacco *et al.*, Multidimensional quantum entanglement with large-scale integrated optics, Science **360**, 285 (2018).

[11] S. P. Walborn, D. S. Lemelle, M. P. Almeida, and P. H. Souto Ribeiro, Quantum Key Distribution with Higher-Order Alphabets Using Spatially Encoded Qudits, Phys. Rev. Lett. **96**, 090501 (2006).

[12] D.-S. Wang, D. T. Stephen, and R. Raussendorf, Qudit quantum computation on matrix product states with global symmetry, Phys. Rev. A **95**, 032312 (2017).

[13] S. Wang, Z.-Q. Yin, H. F. Chau, W. Chen, C. Wang, G.-C. Guo, and Z.-F. Han, Proof-of-principle experimental realization of a qubit-like qudit-based quantum key distribution scheme, Quantum Sci. Technol. **3**, 025006 (2018).

[14] S. Etcheverry, G. Cañas, E. S. Gómez, W. A. T. Nogueira, C. Saavedra, G. B. Xavier, and G. Lima, Quantum key distribution session with 16-dimensional photonic states, Sci. Rep. **3**, 2316 (2013).

[15] Z. Gedik, I. A. Silva, B. Çakmak, G. Karpat, E. L. G. Vidoto, D. de Oliveira Soares-Pinto, F. F. Fanchini *et al.*, Computational speed-up with a single qudit, Sci. Rep. **5**, 14671 (2015).

[16] M. Y. Niu, I. L. Chuang, and J. H. Shapiro, Qudit-Basis Universal Quantum Computation Using $\chi^{(2)}$ Interactions, Phys. Rev. Lett. **120**, 160502 (2018).

[17] H. F. Chau, Quantum key distribution using qudits that each encode one bit of raw key, Phys. Rev. A **92**, 062324 (2015).

[18] N. T. Islam, C. C. W. Lim, C. Cahall, J. Kim, and D. J. Gauthier, Provably secure and high-rate quantum key distribution with time-bin qudits, Sci. Adv. **3**, e1701491 (2017).

[19] R. Pal and S. Bandyopadhyay, Entanglement sharing via qudit channels: Nonmaximally entangled states may be necessary for one-shot optimal singlet fraction and negativity, Phys. Rev. A **97**, 032322 (2018).

[20] M. Agnew, J. Leach, M. McLaren, F. S. Roux, and R. W. Boyd, Tomography of the quantum state of photons entangled in high dimensions, Phys. Rev. A **84**, 062101 (2011).

[21] W. M. Pimenta, B. Marques, T. O. Maciel, R. O. Vianna, A. Delgado, C. Saavedra, and S. Pádua, Minimum tomography of two entangled qutrits using local measurements of one-qutrit symmetric informationally complete positive operator-valued measure, Phys. Rev. A **88**, 012112 (2013).

[22] N. Bent, H. Qassim, A. A. Tahir, D. Sych, G. Leuchs, L. L. Sánchez-Soto, E. Karimi, and R. W. Boyd, Experimental Realization of Quantum Tomography of Photonic Qudits Via Symmetric Informationally Complete Positive Operator-Valued Measures, Phys. Rev. X **5**, 041006 (2015).

[23] T. Ikuta and H. Takesue, Implementation of quantum state tomography for time-bin qudits, New J. Phys. **19**, 013039 (2017).

[24] D. Martínez, M. A. Solís-Prosser, G. Cañas, O. Jiménez, A. Delgado, and G. Lima, Experimental quantum tomography assisted by multiply symmetric states in higher dimensions, Phys. Rev. A **99**, 012336 (2019).

[25] A. J. Gutiérrez-Esparza, W. M. Pimenta, B. Marques, A. A. Matoso, S. Pádua *et al.*, Experimental characterization of two spatial qutrits using entanglement witnesses, Opt. Express **20**, 26351 (2012).

[26] A. J. Gutiérrez-Esparza, W. M. Pimenta, B. Marques, A. A. Matoso, J. Sperling, W. Vogel, and S. Pádua, Detection of nonlocal superpositions, Phys. Rev. A **90**, 032328 (2014).

[27] B. Marques, A. A. Matoso, W. M. Pimenta, A. J. Gutiérrez-Esparza, M. F. Santos, and S. Pádua, Experimental simulation of decoherence in photonics qudits, Sci. Rep. **5**, 16049 (2015).

[28] J. J. M. Varga, L. Rebón, Q. P. Stefano, and C. Iemmi, Characterizing d-dimensional quantum channels by means of quantum process tomography, Opt. Lett. **43**, 4398 (2018).

[29] A. Politi, M. J. Cryan, J. G. Rarity, S. Yu, and J. L. O'Brien, Silica-on-silicon waveguide quantum circuits, Science **320**, 646 (2008).

[30] G. D. Marshall, A. Politi, J. C. F. Matthews, P. Dekker, M. Ams, M. J. Withford, and J. L. O'Brien, Laser written waveguide photonic quantum circuits, Opt. Express **17**, 12546 (2009).

[31] P. J. Shadbolt, M. R. Verde, A. Peruzzo, A. Politi, A. Laing, M. Lobino, J. C. F. Matthews, M. G. Thompson, and J. L. O'Brien, Generating, manipulating and measuring entanglement and mixture with a reconfigurable photonic circuit, Nat. Photon. **6**, 45 (2012).

[32] J. L. O'brien, A. Furusawa, and J. Vučković, Photonic quantum technologies, Nat. Photon. **3**, 687 (2009).

[33] L. Caspani, C. Xiong, B. J. Eggleton, D. Bajoni, M. Liscidini, M. Galli, R. Morandotti, and D. J. Moss, Integrated sources of photon quantum states based on nonlinear optics, Light: Sci. Appl. **6**, e17100 (2017).

[34] B. J. Smith, D. Kundys, N. Thomas-Peter, P. G. R. Smith, and I. A. Walmsley, Phase-controlled integrated photonic quantum circuits, Opt. Express **17**, 13516 (2009).

[35] K. M. Davis, K. Miura, N. Sugimoto, and K. Hirao, Writing waveguides in glass with a femtosecond laser, Opt. Lett. **21**, 1729 (1996).

[36] A. M. Streltsov and N. F. Borrelli, Fabrication and analysis of a directional coupler written in glass by nanojoule femtosecond laser pulses, Opt. Lett. **26**, 42 (2001).

[37] A. Aspuru-Guzik and P. Walther, Photonic quantum simulators, Nat. Phys. **8**, 285 (2012).

[38] A. A. Houck, H. E. Türeci, and J. Koch, On-chip quantum simulation with superconducting circuits, Nat. Phys. **8**, 292 (2012).

[39] N. C. Harris, G. R. Steinbrecher, M. Prabhu, Y. Lahini, J. Mower, D. Bunandar, C. Chen, F. N. C. Wong, T. Baehr-Jones, M. Hochberg *et al.*, Quantum transport simulations in a programmable nanophotonic processor, Nat. Photon. **11**, 447 (2017).

[40] A. J. Kerman, Multiloop interferometers for quantum information processing, US Patent App. 15/354,275, 18 May 2017.

[41] F. Qiu-Bo, Remote preparation of photon polarization states within a network, Chin. Phys. Lett. **25**, 20 (2008).

[42] W. Zhang-Yin, Controlled remote preparation of a two-qubit state via an asymmetric quantum channel, Commun. Theor. Phys. **55**, 244 (2011).

[43] C. Wang, Z. Zeng, and X.-H. Li, Controlled remote state preparation via partially entangled quantum channel, Quant. Info. Proc. **14**, 1077 (2015).

[44] T. B. Cao, B. A. Nguyen *et al.*, Flexible controlled joint remote preparation of an arbitrary two-qubit state via non-maximally entangled quantum channels, Adv. Natural Sci. **7**, 025007 (2016).

[45] C. Schaeff, R. Polster, M. Huber, S. Ramelow, and A. Zeilinger, Experimental access to higher-dimensional entangled quantum systems using integrated optics, Optica **2**, 523 (2015).

[46] M. G. Raymer, M. Beck, and D. McAlister, Complex Wave-Field Reconstruction Using Phase-Space Tomography, Phys. Rev. Lett. **72**, 1137 (1994).

[47] J. P. Home, M. J. McDonnell, D. M. Lucas, G. Imreh, B. C. Keitch, D. J. Szwer, N. R. Thomas, S. C. Webster, D. N. Stacey, and A. M. Steane, Deterministic entanglement and tomography of ion–spin qubits, New J. Phys. **8**, 188 (2006).

[48] M. Riebe, K. Kim, P. Schindler, T. Monz, P. O. Schmidt, T. K. Körber, W. Hänsel, H. Häffner, C. F. Roos, and R. Blatt, Process Tomography of Ion Trap Quantum Gates, Phys. Rev. Lett. **97**, 220407 (2006).

[49] P. Six, Ph. Campagne-Ibarcq, I. Dotsenko, A. Sarlette, B. Huard, and P. Rouchon, Quantum state tomography with non-instantaneous measurements, imperfections, and decoherence, Phys. Rev. A **93**, 012109 (2016).

[50] T. Xin, D. Lu, J. Klassen, N. Yu, Z. Ji, J. Chen, X. Ma, G. Long, B. Zeng, and R. Laflamme, Quantum State Tomography Via Reduced Density Matrices, Phys. Rev. Lett. **118**, 020401 (2017).

[51] J. G. Titchener, A. S. Solntsev, and A. A. Sukhorukov, Two-photon tomography using on-chip quantum walks, Opt. Lett. **41**, 4079 (2016).

[52] J. G. Titchener, M. Gräfe, R. Heilmann, A. S. Solntsev, A. Szameit, and A. A. Sukhorukov, Scalable on-chip quantum state tomography, npj Quantum Inform. **4**, 19 (2018).

[53] D. Oren, M. Mutzafi, Y. C. Eldar, and M. Segev, Quantum state tomography with a single measurement setup, Optica **4**, 993 (2017).

[54] C. Paiva-Sánchez, E. Burgos-Inostroza, O. Jiménez, and A. Delgado, Quantum tomography via equidistant states, Phys. Rev. A **82**, 032115 (2010).

[55] D. Petz and L. Ruppert, Efficient quantum tomography needs complementary and symmetric measurements, Rep. Math. Phys. **69**, 161 (2012).

[56] D. Petz and L. Ruppert, Optimal quantum-state tomography with known parameters, J. Phys. A **45**, 085306 (2012).

[57] A. E. Rastegin, Notes on general SIC-POVMs, Phys. Scr. **89**, 085101 (2014).

[58] J. M. Renes, R. Blume-Kohout, A. J. Scott, and C. M. Caves, Symmetric informationally complete quantum measurements, J. Math. Phys. **45**, 2171 (2004).

[59] S. Barnett, *Quantum Information* (Oxford University Press, Oxford, 2009), Vol. 16.

[60] R. Beneduci, Infinite sequences of linear functionals, positive operator-valued measures and Naimark extension theorem, Bull. London Math. Soc. **42**, 441 (2010).

[61] B. Coecke and É. O. Paquette, POVMs and Naimark's theorem without sums, Electron. Notes Theor. Comput. Sci. **210**, 15 (2008).

[62] R. Beneduci, Unsharpness, Naimark theorem and informational equivalence of quantum observables, Int. J. Theor. Phys. **49**, 3030 (2010).

[63] G. N. M. Tabia, Experimental scheme for qubit and qutrit symmetric informationally complete positive operator-valued measurements using multiport devices, Phys. Rev. A **86**, 062107 (2012).

[64] M. Reck, A. Zeilinger, H. J. Bernstein, and P. Bertani, Experimental Realization of Any Discrete Unitary Operator, Phys. Rev. Lett. **73**, 58 (1994).

[65] W. R. Clements, P. C. Humphreys, B. J. Metcalf, W. S. Kolthammer, and I. A. Walmsley, Optimal design for universal multiport interferometers, Optica **3**, 1460 (2016).

[66] J. Řeháček, B.-G. Englert, and D. Kaszlikowski, Minimal qubit tomography, Phys. Rev. A **70**, 052321 (2004).

[67] W. M. Pimenta, B. Marques, M. A. D. Carvalho, M. R. Barros, J. G. Fonseca, J. Ferraz, M. Terra Cunha, and S. Pádua, Minimal state tomography of spatial qubits using a spatial light modulator, Opt. Express **18**, 24423 (2010).

[68] Z. Chaboyer, T. Meany, L. G. Helt, M. J. Withford, and M. J. Steel, Tunable quantum interference in a 3d integrated circuit, Sci. Rep. **5**, 9601 (2015).

[69] T. Meany, M. Gräfe, R. Heilmann, A. Perez-Leija, S. Gross, M. J. Steel, M. J. Withford, and A. Szameit, Laser written circuits for quantum photonics, Laser Photon. Rev. **9**, 363 (2015).

[70] K. Poulios, R. Keil, D. Fry, J. D. A. Meinecke, J. C. F. Matthews, A. Politi, M. Lobino, M. Gräfe, M. Heinrich, S. Nolte *et al.*, Quantum Walks of Correlated Photon Pairs in Two-Dimensional Waveguide Arrays, Phys. Rev. Lett. **112**, 143604 (2014).